Optimization Method for the Control Law of an Electrical Trimmable Horizontal Stabilizer Actuator Operating at Low Temperatures

MA Haolin, FU Jian and XIA Tianxiang

2023 9th International Conference on Control, Decision and Information Technologies (CoDIT) | 979-8-3503-1140-2/23/$31.00 ©2023 IEEE | DOI: 10.1109/CODIT58514.2023.10284449

***Abstract*— Electrical trimmable horizontal stabilizer actuator (THSA) is a special redundant type of electromechanical actuators (EMA) used for pitch trim in the latest more electric aircraft. It has critical functions and its performance is degraded under extreme operating conditions. This communication proposes a method to optimize the control law of electric THSA to meet the servo control requirements at low temperatures due to various system parameters. The thermal effects of motor winding resistance, permanent magnet flux and mechanical friction were considered in the virtual prototype implemented in the Siemens-AMESim simulation platform. The differential evolution algorithm is used to identify parameters and optimize control laws. A low-temperature experimental rig is built to verify the effectiveness of the optimization method. The results show the good tracking performance and dynamics of control of the electrical THSA at low temperatures.**

Index Terms – THSA, EMA, Temperature effects, Control law optimization, DE algorithm.

I. INTRODUCTION

Improving aircraft fuel efficiency and environmental friendliness are the advanced concepts to push forward more electric aircraft (MEA) and all-electric aircraft (AEA) development in the aerospace industry [1]. Nowadays, typical civil MEA of A350/ B787 and AEA of UAVs are already in service, and electrically actuators of electro-hydrostatic actuators (EHAs) and electromechanical actuators (EMAs) are the new representative application of flight controls, landing gear, braking, etc. [2]. EMAs eliminate both the central and local hydraulic circuits, which brings good maintainability. However, EMAs are not yet mature enough for the primary flight controls of commercial aircraft because of the possibility of jamming malfunctions. Serving Electrical THSA and EMA are similar in terms of power conversion and mechanical transmission, which is the basis for the forward applications of EMAs in the first flight controls and landing gear of the next generation of civil aircraft.

THSA is an important secondary flight control actuator for pitch trimming. In the latest aircraft of A350 and B787, the hydraulically driven THSA have been replaced by electrical types. Some literatures have presented the modelling methods for electrical THSA [3, 4], but few of them focus on thermal analysis, especially on low temperature performance. According to the environmental application standard, the flight control actuators must maintain the servo control response at -55°C. When the temperature drops, the individual components of the electrical THSA have thermal effects, due to the various parameters of the electric motor and mechanical devices, resulting in degradation of control performance if there is no adjustment methodology for the basic control law.

To solve the above challenges, firstly a virtual prototype of electrical THSA was developed in this work that takes temperature effects into account. Then the differential evolution (DE) algorithm is used to identify the parameters and optimize the control law. Finally, the simulation and experimental results are compared.

TABLE I. NOMENCLATURE

Characteristic	Symbol	Unit
Viscous friction coefficient	b_v	$[N/(m/s)]$
Quadratic friction coefficient	b_q	$[N/(m/s)^2]$
The composite friction coefficient of motor, gearbox and nut-screw transmission	b_m, b_g, b_n	$[Nm/(rad/s)]$
Integrated equivalent damping	B_{IE}	$[Nm/(rad/s)]$
Steady-state error	e_{ss}	[-]
Output and aerodynamic force	F_e, F_{ex}	$[N]$
Friction force	F_f	$[N]$
Friction force of nut-screw transmission	F_{fn}	$[N]$
Coulomb force and the Stribeck friction with the breakaway force	F_C, F_b	$[N]$
Mutation constant and crossover constant	F_{sc}, F_{cr}	[-]
Number of generations	G	[-]
Gearbox ratios	i	[-]
Supplied DC and motor current	I_s, I_m	$[A]$
Integrated equivalent inertia	J_{IE}	$[Kgm^2]$
proportional gain and integral gain	K_p, K_i	[-]
Motor torque constant	K_t	$[Nm/A]$
Mass of ball nut	M_s	$[Kg]$
Shape factor	n	[-]
Number of pole pairs	p	[-]
Copper losses	P_{co}	$[W]$
Lead of roller screw	P_h	[mm]
Motor stator winding resistances	R_s	[Ω]
Population Size	S	[-]
Temperature	t	$[°C]$
Rise time	t_r	$[s]$
Motor, gearbox and No-back torque	T_m, T_g, T_b	$[Nm]$
Torque sum of gearbox and No-back	T_n	$[Nm]$
Screw torque	T_e	$[Nm]$
Motor and gearbox friction torque	T_{fm}, T_{fg}	$[Nm]$
DC Supplied and motor armature voltage	U_s, U_m	$[V]$
Command, output and aerodynamic velocity	V_c, V_e, V_{ex}	$[m/s]$
Stribeck velocity	V_S	$[m/s]$
Fitting coefficients	α_0, α_1, α_2, α_3, β_1, β_2	[-]
Efficiency of electric motor	η	[-]
Penalty term coefficients	κ_1, κ_2	[-]
permanent magnet flux linkage	Ψ_{pm}	$[Wb]$
Motor, gearbox and No-back device angular velocity	ω_m, ω_g, ω_b	$[rad/s]$
The composite of gearbox and No-back device angular velocity	ω_n	$[rad/s]$
Screw angular velocity	ω_e	$[rad/s]$

H. MA is with the School of Mechanical Engineering and Automation, Beihang University, Beijing, China (e-mail: ma207185099@gmail.com).

J. FU is with the School of Mechanical Engineering and Automation, Beihang University, Beijing, China (e-mail: fujian@buaa.edu.cn).

T. XIA is with Nanjing Engineer Institute of Aircraft System Jincheng, AVIC, Nanjing, China (e-mail: 283994160@qq.com).

II. VIRTUAL PROTOTYPING OF ELECTRICAL THSA

The architecture of electrical THSA system studied in this paper is shown in Fig. 1, which is designed to be redundant for safety and reliability reasons, which it is the main difference from the conventional EMA. There are two electric motors and motors brakes assembly (MBA) combined in an active/standby dual function. The secondary load path is used to ensure that the driven surface is locked in case a component of primary load path fails (wear or rupture).

While redundant architecture improves the reliability of the flight control actuation system, it also introduces more complexity into the mechanical structure and control requirements. Since the redundancy concepts are activated only in fault mode, the electrical THSA normally functions in the same way as the conventional EMA, so the scheme for the control design could be simplified.

A. Basic Model

The schematic diagram of the functional architecture of the electrical THSA with its control system is shown in Fig. 2. The control theory focuses on the stability, rapidity and accuracy of the system, i.e. overshoot, regulation time and steady-state error. In order to obtain these three characteristics, the actuation system could be linearized to derive its linear transfer function. Therefore, the standby mode path is ignored.

When backup electric motor and secondary load path are disregarded, the architecture of the electrical THSA (apart from No-back device) could be considered as an ordinary EMA. According to the block diagram of EMA linear model [5], the velocity-controlled loop of the linear model of electrical THSA in normal operation mode is shown in Fig. 3.

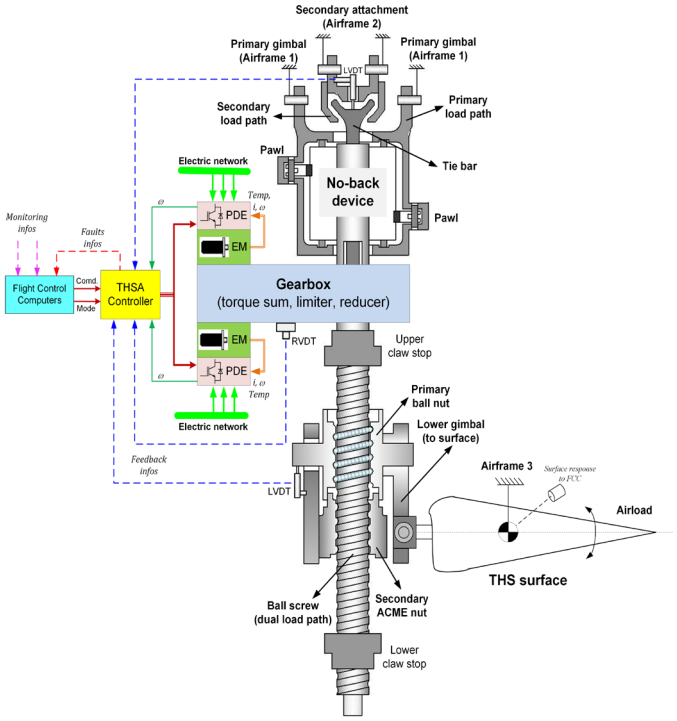

Fig. 1. Scheme of the architecture of electrical THSA for flight control

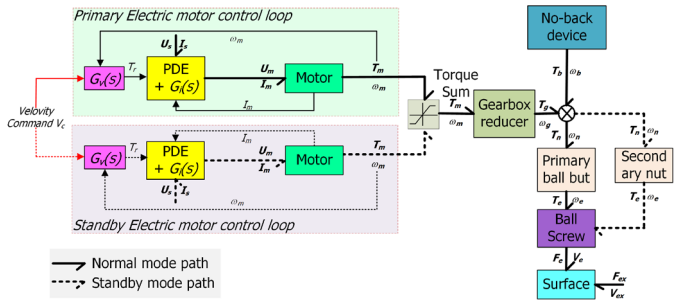

Fig. 2. Functional diagram of the power and signal architecture of electrical THSA.

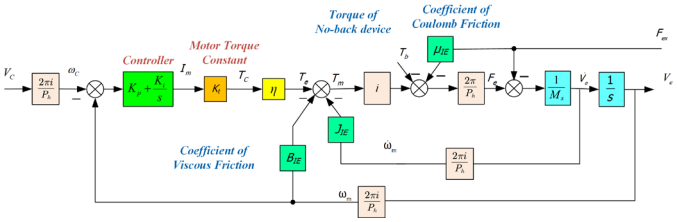

Fig. 3. Block diagram of the linear model of electrical THSA.

Since the THS has a higher load-carrying capacity compared to other aircraft surfaces, the frictional effects cannot be neglected. In the development of the control law, the aerodynamic force F_{ex} is considered as external disturbance and the torque of No-back device is considered as an internal disturbance.

Based on the block diagram of the electrical THSA control (linear model), the velocity controller is used to ensure the rapidity and accuracy of the actuation system. When the other parameters of the linear model are known, the proportional gain K_p and integral gain K_i can be tuned quickly.

B. Temperature Effects of Devices

However, many parameters in Fig. 3, such as η, K_t, B_{IE}, μ_{IE}, are extremely sensitive to temperature, which is a time-varying parameter in the dynamic process. These temperature sensitive parameters exhibit complex correlation with temperature, especially in the freezing environment.

1) Electric Motor Efficiency: There are many power losses in the operation of electric motor. Copper losses are the main source of power losses in electric filed. They are caused by the resistance opposing the current flowing through the stator windings of the motor:

$$U_{co} = I_s R_s \tag{1}$$

$$P_{co} = U_{co} I_s = R_s I_s^2 \tag{2}$$

Influenced by the thermal expansion and contraction of metallic materials, the conductivity of copper conductors decreases with decreasing the temperature, resulting in a decrease in motor rotor resistance.

2) Motor Torque Constant: The motor torque constant is not a parameter with real physical meaning. The motor torque constant of permanent magnets synchronous machine

(PMSM) is related to the permanent magnet flux linkage and the number of pole pairs:

$$T_e = K_t I_m \tag{3}$$

$$K_t = \sqrt{\frac{3}{2}} p \Psi_{pm} \tag{4}$$

The number of pole pairs is invariant in the determination of the electric motor. The flux of the permanent magnet is higher at lower temperature, which results in a small nonlinearity [6].

3) Mechanical Friction: Appropriate modelling of friction is beneficial for control purposes, including identification and compensation. However, friction loss is a very complex phenomenon that is highly dependent on velocity, external load, and temperature. The proposed model for evaluating friction in actuation system modelling and simulation [7].

$$F_f = \left[F_C + b_v |V_r| + b_q V_r^2 + (F_b - F_C) e^{-(|V_r|/V_s)^n} \right] \mathrm{sgn}(V_r) \tag{5}$$

There are six parameters: the Coulomb force F_C, the viscous friction coefficient b_v, the quadratic friction coefficient b_q, the Stribeck friction with breakaway force F_b, the reference Stribeck velocity V_S and the shape factor n. The fourth term on the right-hand side reproduces the Stribeck effect. It affects the actuation system in a narrow range of low velocities.

Also, temperature is generally not considered when modelling friction because it is very complex, although it greatly affects the amount of friction. There are two approaches to how temperature affects the friction force. The first effect results from the increase in fluid viscosity as the temperature decrease, which increases the shear force on the contact medium. The second effect results from the expansion of solids, which can significantly change the effect of preload or breakaway force.

C. Model Implementations

According to the above analysis, the electrical THSA is a complex nonlinear system with coupled mechanical, electrical, thermal and magnetic multiphysics fields. The control law tuned with the linear model is not adapted to the nonlinear effects of temperature. In order to improve the robustness of the electrical THSA system to ambient temperature, a temperature-dependent control law must be designed, i.e., a model with temperature as an input variable is required. The models are developed in the Siemens-AMESim simulation environment, which has a proven track record in the aerospace industry for multiphysics system-level simulation.

The functional model of the electrical THSA in AMESim and the simulation parameters have already been implemented in our previous work [3]. In this work, the redundant architecture is ignored and the temperature interface is introduced. The electric motor, gearbox, nut-screw and no-back device are packaged as supercomponents, and the whole electrical THSA model is shown in Fig. 4.

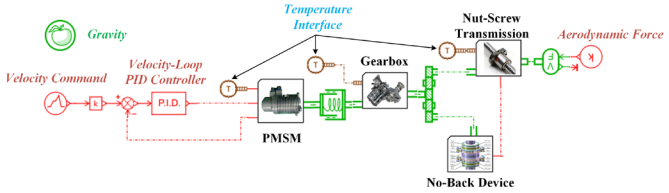

Fig. 4. Functional model of electrical THSA with temperature interface.

III. Parameter Identification and Data Fitting

The modeling process described above is essentially based on the theory of energy transfer and conservation power bond graph theory. Due to the integration of the temperature interface, the electrical THSA model is a "parametric model". The accuracy of the model needs to be verified. Meanwhile, the electrical THSA system is a complex nonlinear system with many system parameters, and some of the system parameters drift with temperature in the low temperature environment. Although the process of drifting the temperature-sensitive parameters with temperature is generally a slow changing process, the model accuracy is inevitably reduced significantly in the case of large temperature differences. It is necessary to estimate the parameters of typical temperature points according to certain system parameter identification methods based on the low-temperature simulation data of the system, and interpolate the corresponding parameters between typical temperature points to ensure the high accuracy of the model at each temperature point.

A. Process of Parameter Identification

The model parameters are mainly identified by the parameters of the electric motor, gearbox and nut-screw. The identification method is based on the iterative optimization of the model based on the actual measured data of the low-temperature experimental rig (for detailed information, see IV.B). The same input signal (velocity ramp signal, anti-drive step signal, etc.) is fed to the low-temperature experimental rig and electrical THSA model. At room temperature, the simulation output data and the experimental output data are largely in agreement.

The differences between the simulation output data and experimental output data increase because some temperature-sensitive parameters drift with decreasing the temperature. The identification algorithm adjusts the model parameters based on the model and experimental output error:

$$J(\theta) = \sum_{k=1}^{N} f(e(k)) \tag{6}$$

where $f(\cdot)$ is a function of $e(k)$, which is an error function defined on the interval (0, N) and refers to the error between the model and the actual system.

After a certain number of iterations, the electrical THSA model gradually converges to the final model, which differs little from the actual system. The whole process is shown in Fig. 5.

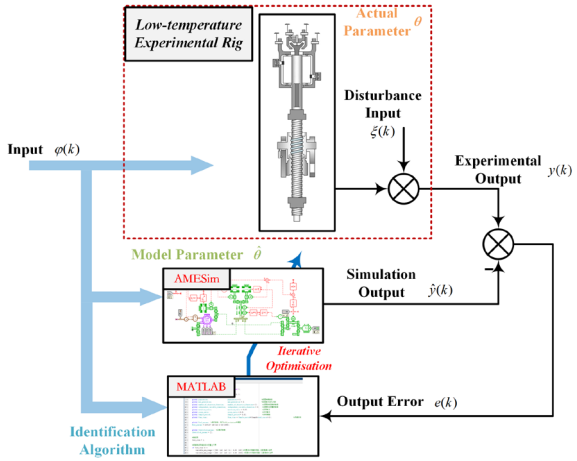

Fig. 5. Process of model parameter identification.

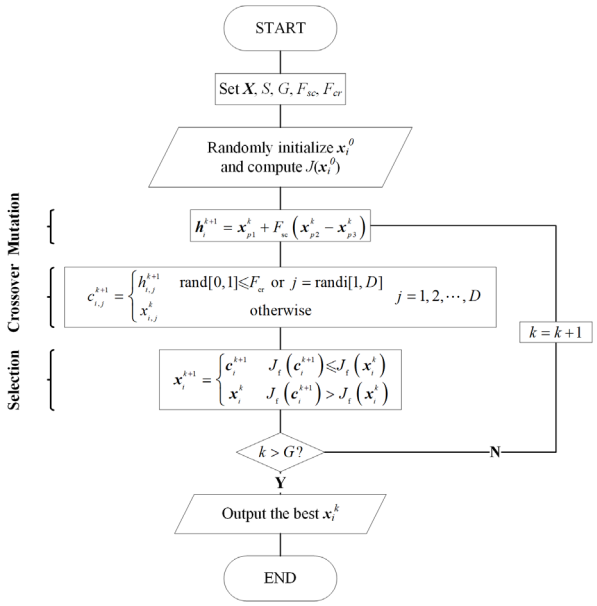

Fig. 6. Flow chart of DE algorithm for parameter identification.

B. Identification Algorithm

Since the electrical THSA model does not take the form of linear equations, least squares identification cannot be used for the functional model in AMESim. The DE algorithm is a heuristic algorithm based on differential mutation and is real-coded. Its compact structure, high convergence rate, and simple yet powerful and straightforward properties make it an ideal candidate for parameter optimization [8]. By setting the optimization objective function to (6), the DE algorithm can be applied to parameter identification of complex nonlinear systems with non-differentiable, multiple polarization points and high dimension.

The flow of the DE algorithm for parameter identification is shown in Fig. 6. Initialize the problem dimension $\boldsymbol{X}$, population size $S = 45$, number of generation $G = 30$, mutation constant $F_{sc} = 0.16$ and the crossover constant $F_{cr} = 0.5$. Through mutation, crossover, and selection steps, the best individual is selected. The DE algorithm was finally implemented programmatically in MATLAB.

C. Identification Result Analysis

The system-level functional model of the electrical THSA is inadequate for identification because of its numerous parameters. Therefore, the system-level model is functionally decomposed into supercomponents.

1) Electric motor (PMSM): The electromagnetic and mechanical friction characteristics of the PMSM are both affected by temperature. These include the rotor resistance, the flux linkage of the permanent magnet, Coulomb torque and the viscous friction coefficient, which have the greatest influence on the motor performance.

The error of the stator current on the q-axis between the outputs of simulation and experimental is the objective function of the DE algorithm, since the error of rotor speed is mainly influenced by the speed control loop. There are eight data sets for temperature points at 25℃, 0℃, -10℃, -20℃, -30℃, -40℃, -50℃ and -55℃. The four data fitting functions and their fitting coefficients are summarized in Table II.

It is interesting to note that all the fitting functions are 2nd or 3rd order linear functions, except for the fitting function of Coulomb torque, which is a 2nd order exponential fitting, which means that the relationship between the Coulomb torque of PMSM and temperature is a complex nonlinear relationship.

2) Gearbox: The gearbox focuses only on the mechanical friction characteristics. The relationship between the friction torque of the gearbox and the temperature and speed is shown in Fig. 7.

TABLE II. DATA FITTING FUNCTIONS AND FITTING COEFFICIENTS OF ELECTRIC MOTOR.

	Fitting functions	Fitting coefficients			
		α_3 / β_2	α_2	α_1	α_0 / β_1
R_s	$R_s(t) = \alpha_3 t^3 + \alpha_2 t^2 + \alpha_1 t + \alpha_0$	-5e-6	7e-5	3e-2	1.2
Ψ_{pm}	$\Psi_{pm}(t) = \alpha_2 t^2 + \alpha_1 t + \alpha_0$		-4e-6	6e-5	0.1
T_{fm}	$T_{fm}(t) = \alpha_1 e^{\beta_1 t} + \alpha_2 e^{\beta_2 t}$	9e-3	3e-2	1e-2	-4e-2
b_m	$b_m(t) = \alpha_3 t^3 + \alpha_2 t^2 + \alpha_1 t + \alpha_0$	1e-10	1e-8	2e-8	4e-5

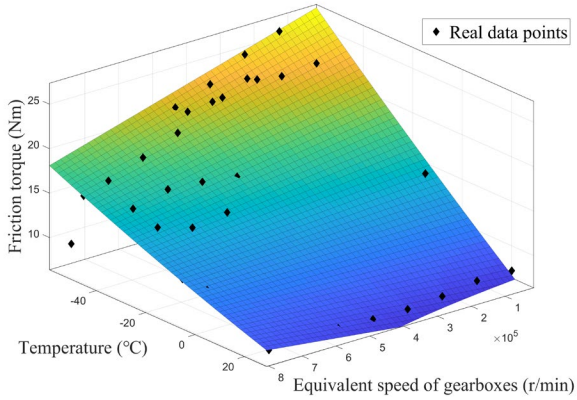

Fig. 7 Friction as a function of temperature and speed fitted surface plots for gearbox.

There are eight sets of temperature experiments with eight different velocity specifications at each temperature, for a total of 64 data points. From the trend of the surface plot in Fig. 9, it can be seen that the friction torque is higher at low temperatures and low speeds, which means that the viscous friction coefficient plays a negative role. The specific fitting functions and their fitting coefficients are summarized in Table III.

3) Nut-screw transmission: The nut-screw has the same temperature-dependent parameters as the gearbox, which are Coulomb force and the viscous friction coefficient. The relationship between the friction force of the nut-screw and the temperature as well as linear velocity is shown in Fig. 8.

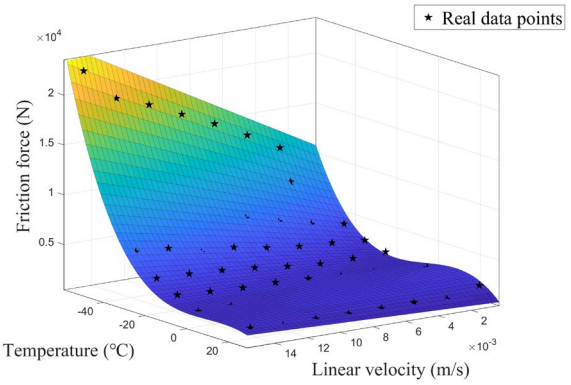

Fig. 8. Friction versus temperature and linear speed fitted surface plots for nut-screw transmission.

TABLE III. DATA FITTING FUNCTIONS AND FITTING COEFFICIENTS OF GEARBOX AND NUT-SCREW.

	Fitting functions	Fitting coefficients			
		α_3	α_2	α_1	α_0
T_{fg}	$T_{fg}(t)=\alpha_3 t^3+\alpha_2 t^2+\alpha_1 t+\alpha_0$		2e-4	-0.25	11
b_g	$b_g(t)=\alpha_1 t+\alpha_0$			1.8e-7	-6e-7
F_{fn}	$F_{fn}(t)=\alpha_3 t^3+\alpha_2 t^2+\alpha_1 t+\alpha_0$	-0.07	-1.4	37	2.7e3
b_n	$b_n(t)=\alpha_2 t^2+\alpha_1 t+\alpha_0$		230	-3e3	4e4

The difference is that the friction force is higher at low temperature and high linear speed. The intriguing difference between rotating mechanical parts and linearly moving mechanical parts is worth investigating in depth in conjunction with specific experimental data. The specific fitting functions and their fitting coefficients are summarized in Table III.

IV. OPTIMIZATION OF CONTROL LAW

The electrical THSA controller uses a dual PI controller with outer velocity and inner current loops. The current loop control law is built into the power drive electronics (PDE) of electric motor and is set by the PDE, so no adjustment is required. By optimizing the proportional gain K_p and the integral gain K_i of the velocity loop, the electrical THSA achieves a command with a small speed tracking error.

A. Automatic Optimization

For engineering applications, PID parameters are usually set manually by engineers based on their experience. This method requires experimental verification by engineers after each adjustment of the control law, which is time consuming and inefficient. An automatic control law optimization based on a functional model is presented.

The control law optimization process uses LabVIEW, MATLAB and AMESim as platforms and data interaction between the programmers. MATLAB is used as the main platform for running the optimization algorithm and receives the optimization instructions and experimental temperature and load data from LabVIEW. The model in AMESim is called by batch runs and iteratively fitted by the global optimization search algorithm until the objective function converges to obtain the optimal control law.

The entire optimization process is highly automated and uses the same DE algorithm (modify the objective function):

$$\min \quad J(\theta)=\sum_{k=1}^{N}\frac{1}{2}(v-\hat{v})^2+\kappa_1 t_r+\kappa_2 e_{ss} \tag{7}$$

In addition to integrating the individual errors of the experimental and the simulated velocity outputs, the rise time and steady-state error of the velocity profile are included as penalty terms in the objective function. The global optimization capability of the DE algorithm ensures that the optimization results are less likely to fall within the local optimum.

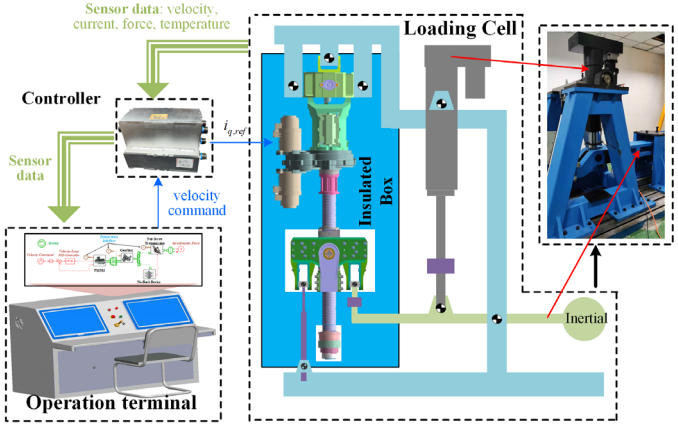

Fig. 9. The low-temperature experimental rig for electrical THSA.

B. Description of the Low-temperature Experimental Setup

As shown in Fig. 9, a low-temperature experimental setup is built to verify the experiments. A load cell is used to exert a desired aerodynamic force for the electrical THSA. Trim speed control and load control are performed by corresponding controllers based on command signals from the operator terminal and sensor data. Nine platinum resistance temperature detectors are arranged internally to measure the temperature of various parts of the body. All test results are available in the operator terminal for operators.

Four types of experiments were conducted with this low-temperature experimental rig: 1) experiments with the motor unloaded (separate tests), 2) experiments with the motor disconnected under anti-driven load, 3) experiments with both

the motor and the gearbox disconnected under anti-driven load, 4) experiments with the driven load. The results of the first three experiments are used for the previous parameter identification, and the last experiment is used to test the performance of the control law optimization.

C. Result Analysis

1) Identification Result: A velocity ramp demand v_c equals 9mm/s for the flight surface is applied with an acceleration of 30mm/s^2. At the same time, the load cell applies a constant force of 55kN and the temperature in the isolated box is -30°C. The velocity curve and the current curve are shown in Fig. 10 with the same control law.

The velocity error is 0.78% and the current error is 3.56%, which proves that the functional model of the electrical THSA has a high degree of accuracy. This model could be used to optimize the control law without the need for multiple experimental tunings at each temperature.

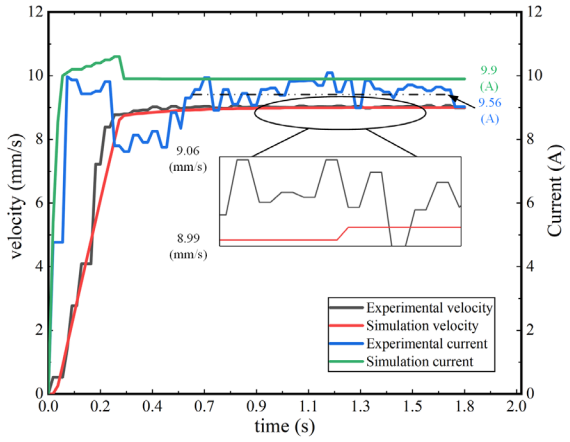

Fig. 10. Simulation response of surface position in different model levels.

2) Optimization Result: The control law before optimization is tuned at 25°C, which is not suitable at -30°C. The same experimental conditions as before are given and the control law is summarized in Table IV.

During the iterative process of control law optimization, it is interesting to note that the population gradually converges linearly, that is, the ratio of K_p and K_i gradually converges to a constant value of 0.1218, which provides a reference for the subsequent control law optimization.

The velocity curve before optimization and after optimization is shown in Fig. 11. The set rise time is 0.3s and the rise time decreases from 0.45s to 0.32s after optimization. The steady state error decreases from 0.0022 to -0.00013 after optimization.

TABLE IV. THE CONTROL LAW AND ITS INDICATORS BETWEEN BEFORE OPTIMIZATION AND AFTER OPTIMIZATION.

Before Optimization				**After Optimization**			
Control law		Indicators		Control law		Indicators	
K_p	K_i	t_r	e_{ss}	K_p	K_i	t_r	e_{ss}
0.12	0.45	0.42s	0.0022	0.363	2.98	0.32s	-0.00013

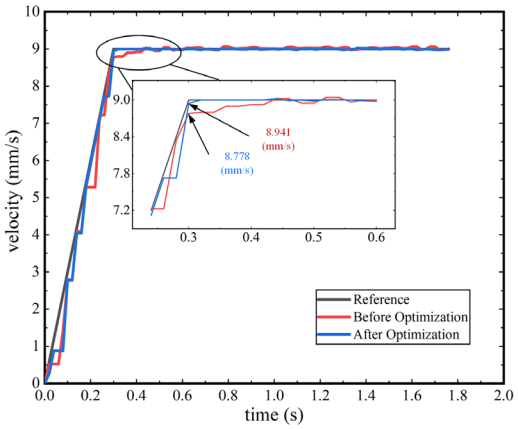

Fig. 11. Speed curve between before optimization and after optimization.

V. CONCLUSION

A control law optimization methodology was proposed to support the analysis of the electrical THSA performance considering thermal effects, especially at low temperatures. The optimization methodology could help engineers efficiently tune the control law of actuation system in aerospace application. The effects of low temperatures on the electric motor and mechanical devices, including launch capability, electric residence, electromagnetic flux, and mechanical friction, were considered. Finally, an experimental rig was developed to verify the effectiveness of the proposed control law tuning method by the real time experiments.

REFERENCES

[1] M. Lukic *et al.*, "State of the Art of Electric Taxiing Systems", in *2018 IEEE International Conference on Electrical Systems for Aircraft, Railway, Ship Propulsion and Road Vehicles & International Transportation Electrification Conference (ESARS-ITEC)*, Nottingham, pp. 1–6, 2018.

[2] P. Giangrande *et al.*, "Considerations on the Development of an Electric Drive for a Secondary Flight Control Electromechanical Actuator", *IEEE Trans. on Ind. Applicat.*, vol. 55, no. 4, pp. 3544–3554, 2019.

[3] W Zhan, J Fu et al., "Investigations on MBSE Modelling and Dynamic Performance Assessment of an Electrical Trimmable Horizontal Stabilizer Actuator", *Chinese Journal of Aeronautics*, 2023[Acceptance].

[4] J. Fu, C. Zheng, J.-C. Maré *et al.*, "Virtual prototyping of electrical THSA focused on mechanical power transmission functions", in *32nd Congress of the International Council of the Aeronautical Sciences, Shanghai, China*. 2021.

[5] J. Fu, I. Hazyuk, and J.-C. Maré. "Preliminary Design Rules for Electromechanical Actuation Systems–Effects of Saturation and Compliances", *5th European Air and Space Conference, Delft, Netherlands.* 2015.

[6] S. Xiao and A. Griffo, "PWM-Based Flux Linkage and Rotor Temperature Estimations for Permanent Magnet Synchronous Machines", *IEEE Trans. Power Electron.*, vol. 35, no. 6, pp. 6061–6069, 2020.

[7] J.-C. Maré, "Friction modelling and simulation at system level: a practical view for the designer", *Proceedings of the Institution of Mechanical Engineers, Part I: Journal of Systems and Control Engineering*, vol. 226, no. 6, pp. 728–741, 2012.

[8] M. S. Saad, H. Jamaluddin and I. Z. M. Darus, "Implementation of PID controller tuning using differential evolution and genetic algorithms", *International Journal of Innovative Computing, Information and Control*, vol. 8, no. 11, pp. 7761–7779, 2012.